Diamond Jet Hybrid HVOF Thermal Spray: Rule-Based Modeling of Coating Microstructure

Dan Shi, Mingheng Li, and Panagiotis D. Christofides*

Department of Chemical Engineering, University of California, Los Angeles, California 90095-1592

This paper focuses on the computational modeling and simulation of the microstructure of coatings produced by an industrial high-velocity oxygen-fuel (HVOF) thermal spray process (Diamond Jet hybrid gun, Sulzer Metco, Westbury, NY). On the basis of an understanding of the coating structure and mechanisms of pore formation inside of the coating obtained from experimental studies, a stochastic simulation procedure is used to explore the evolution of the microstructure of the coatings. In the coating growth model, the velocity, temperature, and degree of melting of the particles hitting the substrate are determined by a previously developed mathematical model (first article of this series) describing gas and particle behavior, and the complex characteristics of the thermally sprayed coatings are captured by applying certain basic rules that encapsulate the main physical features of the deposition process. In addition to providing useful insight into pore formation and coating growth, the model is used to make a comprehensive parametric analysis, which allows us to systematically characterize the influence of operating conditions, such as the gas flow rate and spray distance, as well as the effect of particle size, on the particle melting behavior, coating porosity, surface roughness, and deposition efficiency. A comparison of simulation results and experimental studies shows that the proposed model can reasonably predict the relationship between the macroscopic processing conditions and the coating microstructure.

1. Introduction

The thermal spray technique represents a series of particulate deposition processes in which the particles are heated and propelled in a gas/plasma stream to hit a substrate, forming a thin layer of dense, hard and lamellar-structured coating. Since its development in the early 20th century, the thermal spray technology has been one of the most cost-efficient means of protecting substrate surfaces, via coating deposition, from wear, corrosion, and erosion. The 1980s witnessed the invention of the so-called high-velocity oxygen-fuel (HVOF) thermal spray technology, which was a major achievement in the thermal spray industry.[1] Featured with a high gas/particle velocity and a relatively low gas/particle temperature when compared with plasma spraying, HVOF thermal spray is a powerful tool for the fabrication of coatings of metals, cermets, and composites. On one hand, the extremely high particle velocity helps to densify the coating and to increase the deposition rate. On the other hand, the very short residence time in the relatively low-temperature gas flame makes the powder particles highly plastic and prevents superheating or vaporization.[2−5] At present, the HVOF thermal spray has carved out a special niche in the thermal spray industry, particularly in the deposition of nanostructured coatings, because the nanocrystalline structure of the powder particles can be preserved during flight.[2]

To improve coating repeatability and process performance, much experimental work has been done in the past decade to study the effects of key process parameters, such as the gas flow rate, fuel/oxygen ratio, and spray distance, on the physical and mechanical properties of HVOF thermally sprayed coatings.[6−12] The optimization of process parameters involved in these works relies on the conventional Taguchi method, which uses a set of orthogonal arrays that stipulates the manner of conducting the minimal number of experiments that can provide full information on all of the factors affecting the coating performance parameters.[7] This approach is expensive but reliable for a specific HVOF thermal spray process. However, the lack of a fundamental understanding of the dynamics of the gas and particle behavior, as well as of the microscopic deposition process, significantly restricts the applicability of such an approach because the experimentally derived "optimal" solution can be questionable when it is applied to another thermal spray process in which some important parameters, such as the nozzle configuration, powder or fuel type, etc., are different.[2] Mathematical modeling, on the other hand, provides an efficient and versatile alternative to quantify the effect of each of the key process parameters on the coating properties.

In the past decade, significant efforts have been made to simulate the evolution of coating microstructures using mathematical models. For example, stochastic simulation has been applied to model the stochastic deposition and coating growth process in plasma spray.[13−15] These stochastic models are based on certain rules that govern splat formation, coating growth, and pore formation. Parametric analyses have been performed using these models to study how the coating microstructure and physical properties, such as porosity and roughness, are affected by various process parameters, including the gun scanning velocity, spray angle,[13] particle size, gas temperature, and velocity.[14] However, the profiles of the particle temperature, velocity, and degree of melting in the plasma spray process are very

* To whom correspondence should be addressed. Tel.: (310)-794-1015. Fax: (310)206-4107. E-mail: pdc@seas.ucla.edu.

10.1021/ie030560h CCC: $27.50
Published on Web 01/03/2004

different from the corresponding profiles in the HVOF thermal spray, and thus, these models cannot be used to predict the coating microstructure in the HVOF thermal spray process. Recently, continuum-type and stochastic models have been developed to simulate the coating microstructure formation[16,17] in the HVOF thermal spray process; continuum-type models involve partial differential equations governing particle deformation and spreading. However, in these works, the particles at the point of impact on the substrate are assumed to be fully melted, and the important effect of the degree of particle melting (most particles hit the substrate in a semimolten state) is not taken into account in the heat balance that describes the evolution of the particle temperature and the formation of the coating microstructure.

To develop a methodology to precisely control the coating micro- or nanostructure, and thereby the coating mechanical and physical properties, by manipulating macroscale operating conditions, the link between the macroscopic operating conditions and the coating microstructure must be established, and the relationship between the particle size and melting behavior and the coating porosity needs to be understood. In this article, we focus on the modeling of the microstructure of coatings produced by an industrial HVOF thermal spray process (Diamond Jet hybrid gun, Sulzer Metco, Westbury, NY). On the basis of an understanding of the coating structure and mechanisms of pore formation inside the coating obtained from experimental studies,[18−20] stochastic simulations are used to explore the microstructure evolution behavior of the coatings on the substrate. In the coating growth model, the velocity, temperature, and degree of melting of the powders hitting the substrate are determined by a previously developed mathematical model describing gas and particle behavior,[21] and the complex characteristics of the thermally sprayed coatings are captured by applying several basic rules that encapsulate the main physical features of the deposition process. In addition to providing useful insight into the pore formation and coating growth, the model is used to perform a comprehensive parametric analysis, which allows us to systematically characterize the influence of operating conditions, such as the gas flow rate and spray distance, as well as the effect of particle size, on the particle melting behavior, coating porosity, surface roughness, and deposition efficiency. A comparison of simulation results and experimental studies shows that the proposed model can provide good predictions of the relationship between the macroscopic processing conditions and the coating microstructure.

2. Characteristics of Deposition and Coating Growth

Thermally sprayed coatings consist of lamellar splats interspersed with pores. The splats, which are the fundamental building blocks of the coating, are formed by the impact, deformation, spreading, and solidification of individual droplets. The pores, however, are formed by the interaction of the droplets and the previously deposited coating surface. In this section, several characteristics involved in the deposition and coating growth process, including deformation, pore formation, and surface roughness, are described.

2.1. Deformation. In the HVOF thermal spray process, each individual particle is accelerated and heated in a burning gas flame, after which it impinges on the substrate in a molten, partially molten, or solid state. At impact, the sudden stagnation of the powder particles leads to a pressure buildup at the particle−surface interface, and deformation occurs. As the particles splash on the substrate, they are also quenched to the substrate temperature in a very short time. For the particle deformation process, if a particle is fully melted, it is assumed that the droplet becomes a cylinder as a result of deformation[22] (see Figure 1a). The splat flattening degree ξ is defined by the equation

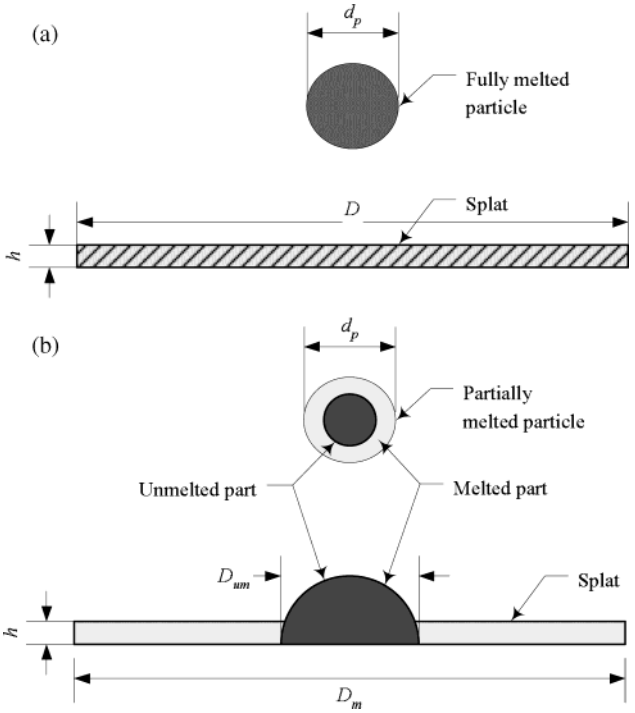

Figure 1. Deformation of fully melted particle and partially melted particles upon impact on the substrate.

$$\xi = \frac{D}{d_p} = \frac{2}{d_p}\sqrt{\frac{A}{\pi}} \tag{1}$$

where D and A are the estimated diameter and area, respectively, of the splat and d_p is the particle diameter prior to impact. The analysis of Madejski[22] shows that ξ depends on several dimensionless parameters characterizing the impact and spreading processes, including the Reynolds number ($Re = d_p v_p/\nu_p$, where ν_p is the kinematic viscosity of the droplets), which represents the viscous dissipation of the inertia forces; the Weber number ($We = d_p v_p^2 \rho_p/\sigma_p$, where σ_p is surface tension of the droplets), which quantifies the conversion of the kinetic energy into surface energy; and the Peclet number ($Pe = v_p d_p/\epsilon_p$, where ϵ_p is the thermal diffusivity of the solidified layer), which expresses the freezing rate.[22] Under the operating conditions typically employed in the HVOF thermal spray process, solidification is insignificant before deformation is complete, and therefore, the flattening ratio can be expressed as a function of We and Re as follows[22]

$$\frac{3\xi^2}{We} + \frac{1}{Re}\left(\frac{\xi}{1.2941}\right)^5 = 1 \tag{2}$$

The above equation is valid for $We > 100$ and $Re > 100$. When the surface tension effects are negligible, which

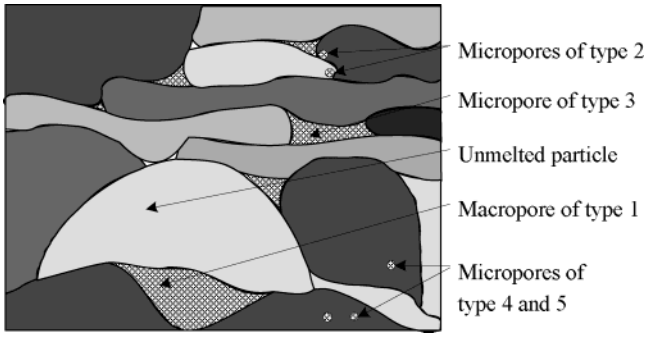

Figure 2. Schematic of the five types of pores.

is usually true for particles larger than 10 μm, eq 2 can be further simplified to

$$\xi = 1.2941 Re^{0.2} \tag{3}$$

If a particle is partially melted, our modeling procedure assumes that the unmelted part will form a hemisphere with the equivalent volume and the melted part will form a ring around this hemisphere (see Figure 1b), whose flattening ratio can be calculated using the same formula.

2.2. Pore Formation. Porosity, which is defined as the ratio of the volume of the pores inside the coating to the total volume of the coating, is one of the most important quality parameters of the coatings produced by the HVOF thermal spray process. Experimental studies have shown that a lamellar microstructure is consistently observed on cross sections of a coating, and pores are distributed in the lamellar structure, regardless of the processing conditions.[1] However, the amount, size, and distribution of pores in thermally sprayed coatings are dependent to a large extent on the processing conditions. These variables, which significantly affect the thermal conductivity and mechanical properties of the coatings, can be controlled more efficiently if an in-depth understanding of the fundamental mechanisms of porosity formation is established. In this sense, estimation of the coating porosity is one of the main objectives of this work.

Liu et al.,[18−20] on the basis of their experimental investigations, proposed several possible mechanisms of pore formation in the coating microstructure. Five major types of pores are classified (see Figure 2). The first one is a macropore type, whose size is comparable to the droplet size. Such pores are primarily formed in the vicinity of solidified, unmelted, or partially melted particles as a result of the unfree spreading of subsequent droplets around these slightly flattened particles (mechanism 1). The remaining four types of pores are all of micropore type, with sizes that are much smaller than the size of the droplets. Specifically, they are formed by (2) the solidification of voids caused by droplet/droplet and droplet/liquid-surface-layer interactions, (3) the separation of liquid from the solid/liquid interface or liquid ejection or rebounding (detached liquid can entrap voids), (4) the presence of cavities in droplets before impact, and (5) extraneous inclusions and dispersoids (e.g., carbides, nitrides, and oxides) that might be present in droplets. The occurrence of each mechanism depends on the processing conditions. For example, when the degree of melting of the particles at impact is low and there are many solid particles in the sprayed powder at the point of impact on the substrate, the first two mechanisms are dominant. When the deposition layers are thin and the resultant rate of heat extraction in the deposited material is high, mechanism 3 becomes important. If a large number of extraneous particles are present in the droplets, mechanism 5 will be significant. Because the spray powder used in the current study is nickel, the powder particles are dense, and it can be assumed that there is no reaction of carbides or oxides inside them. Therefore, pores formed by mechanisms 4 and 5 can be neglected. Mechanisms 1−3 are included in the microstructure model, and their relative importance varies depending on the operating conditions.

2.3. Surface Roughness. The roughness of a coating surface is another important factor that affects coating quality. A smooth surface can enhance the coating performance in terms of abrasion, wear, and corrosion resistance. In this work, the roughness is defined as the arithmetic mean of the absolute difference between the surface height of each grid and the average surface height

$$R_a = \frac{\sum_{i=1}^{n} |h(i) - h_m|}{n} \tag{4}$$

where R_a is the roughness, n is the number of grid points used in the model, $h(i)$ is the surface height of grid point i, and h_m is the average surface height calculated by using the expression $\sum_{i=1}^{n} h(i)/n$.

The surface roughness is primarily dependent on the substrate properties as well as the particle size and chemical and physical states of the particles at the point of impact on the substrate. This work considers the substrate to be smooth and neglects the effect of the roughness of the substrate on the coating properties. However, it should be noted that the substrate surface is usually roughened before the coating processing. Such a treatment can increase the bonding strength between the thermally sprayed coating and the substrate. Mellali et al.[23] have concluded that the particle adhesion/cohesion on the surface increases with substrate roughness, at least for the well-molten particles.

3. Computer Simulation of Coating Formation

Because of the polydisperse nature of the powder size distribution and the stochastic nature of the deposition process, a stochastic simulation method, which is based on random number generation and rule-based modeling, is used to explore the particle behavior in the deposition and coating formation processes. In this section, the modeling procedure, coating growth rules, and model settings are presented. Although the proposed model is applied here to a coating sprayed by the Diamond Jet hybrid HVOF thermal spray process, the modeling methodology is applicable to coatings sprayed with other HVOF thermal spray processes.

3.1. Simulation Procedure. The procedure followed for the simulation of the coating microstructure is based on the sequential modular method, which is diagrammed in Figure 3. At the beginning of each simulation run, the process operating conditions (such as the mass flow rates of oxygen, fuel, and air) and the particle size distribution parameters are specified. After the initialization, the simulation repeats a process in which individual particles hit the surface of the coating until

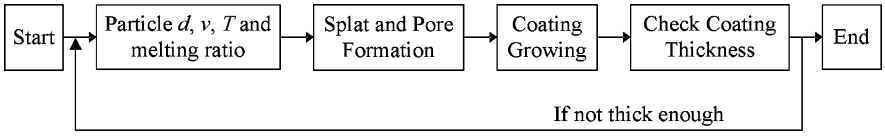

Figure 3. Modeling procedure.

the coating thickness reaches the desired set-point value. The size of each particle is chosen by using a random number generator according to a log−normally distributed particle size distribution of the following form[30]

$$f(d_p) = \frac{1}{\sqrt{2\pi}\sigma d_p} \exp\left[-\frac{(\ln d_p - \mu)^2}{2\sigma^2}\right] \tag{5}$$

where $f(d_p)$ is the size distribution function and μ and σ^2 are two dimensionless parameters corresponding to the mean and the variance, respectively, of ln d_p, which obeys a normal distribution. For particles that are log−normally distributed, μ and σ can be determined by the formulas[5]

$$\mu = \ln \sqrt[3]{d_{10}d_{50}d_{90}} - 1.831\left(\ln\sqrt{\frac{d_{90}}{d_{10}}}\right)^2$$
$$\sigma = 0.781 \ln \sqrt{\frac{d_{90}}{d_{10}}} \tag{6}$$

where d_{10}, d_{50}, and d_{90} are three characteristic diameters that can be obtained experimentally.[29]

Once the particle size is determined, the particle velocity, temperature, and melting ratio at the point of impact on the substrate are calculated by using the HVOF thermal spray process model developed in the first article of this series.[21] The hitting position of the particle on the substrate is also determined by two independent random numbers. The program then simulates how each individual particle hits the substrate and forms a splat. For the simulation of splat accumulation, we consider the coating formation process to be a sequence of independent discrete events of each individual particle hitting the previously formed coating layer. After all of the parameters of a particle prior to hitting the previously deposited coating layer, such as the melting ratio, flattening ratio, etc., are determined, the particle is added to the already-formed coating layer according to certain rules, which are discussed in subsection 3.2 below. When the coating thickness reaches its set-point value, the program saves the configuration of the simulated coating section and calculates the coating porosity, surface roughness, and deposition efficiency. The deposition efficiency is defined as the ratio of the volume of the particles deposited on the substrate to the total volume of particles sprayed by the HVOF process.

To increase the efficiency of the computation, the model simulates only the cross section of the coating that is perpendicular to the substrate, i.e., it simulates coating growth in two dimensions. The point of impact of a particle on the substrate is determined by two random variables, corresponding to its two-dimensional position on the coating surface. The first one represents the position in the x coordinate (x_p), calculated from a reference point on the simulated section to the center of the splat. The second represents the position in the y coordinate (y_p), calculated from the position where the splat is cut by the cross section to the center of the splat (see Figure 4). Specifically

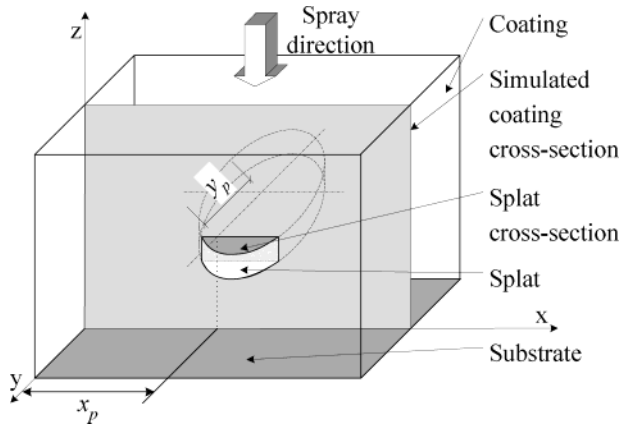

Figure 4. Sketch of the splat position used in the model.

$$x_p = uL + L/2$$
$$y_p = wD \tag{7}$$

where u and w are two independent and uniformly distributed random variables in the interval [−0.5, 0.5], L is the length of the simulated coating section, and D is the diameter of the splat. Note that uniformly but not normally distributed variables are used to describe the splat position because the thermal spray gun can generally move back and forth. After the point of impact of a particle on the substrate is determined, the splat is added to the previously deposited coating layer, and pores might be formed, depending on the conditions of the previously deposited coating layer.

3.2. Coating Growth Rules. Several different events might take place when a particle hits the substrate. The occurrence of each event depends on the physical state of the sprayed particle and the conditions of the previously deposited layer at the impact point. The rules governing the geometric shape of the splats and the formation of the pores are described as follows:

1. If a particle at the point of impact on the substrate is partially melted, the unmelted part will form a hemisphere on the previously deposited layer, and the melted part will form a ring around this hemisphere (see Figure 1b). Furthermore, if the unmelted part of the particle hits at the point of the previously deposited layer that is formed by an unmelted particle, it will bounce off, and a hole will be formed in the center of the disk. Otherwise, the hemisphere hits the surface, and macrosize pores might form under the hemisphere. Figure 5a and b shows the coating layer before and after a partially melted particle hits the surface. This figure illustrates the formation of one pore as the unmelted particle covers the gap. This kind of pore formation is

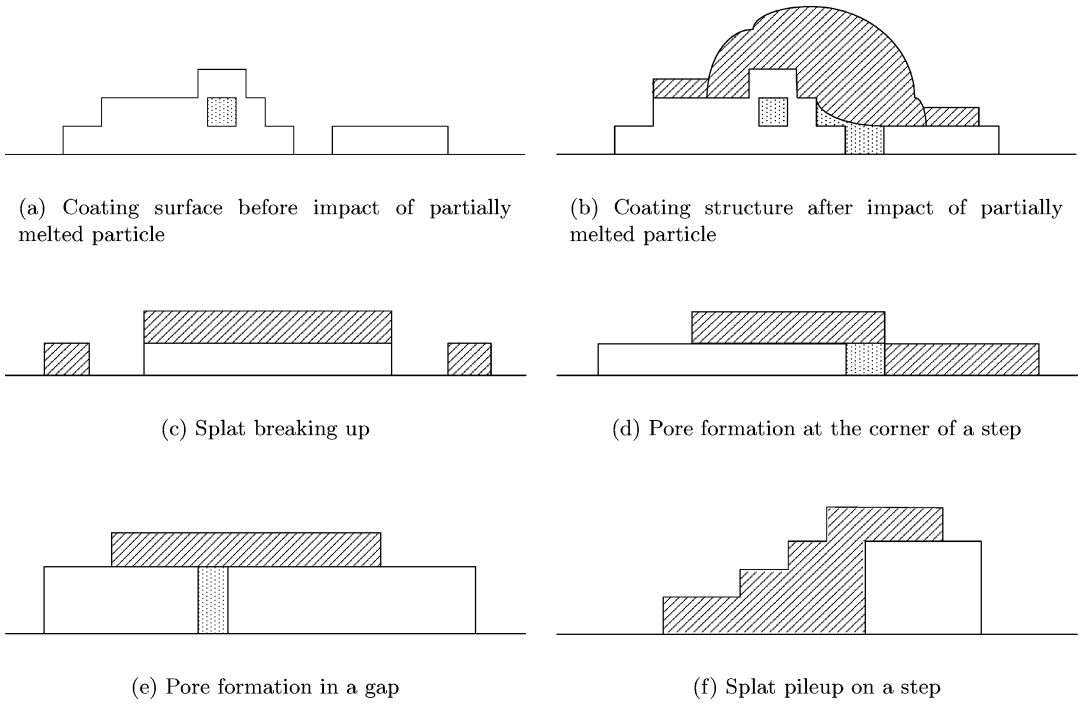

(a) Coating surface before impact of partially melted particle

(b) Coating structure after impact of partially melted particle

(c) Splat breaking up

(d) Pore formation at the corner of a step

(e) Pore formation in a gap

(f) Splat pileup on a step

Figure 5. Splat formation rules. (The shaded area corresponds to the added splat, and the dotted area corresponds to pore formation.)

consistent with the first type of pore formation mentioned in subsection 2.2.

2. When a particle hits the substrate, the melted part fits on the surface as much as possible. After the impact region of the particle fits on the surface, the splat spreads outward without forming a new pore. The impact region is determined by the size and the cross-sectional position of the particle.

3. During splat spreading, if the splat comes to a vertical drop, the program calculates the ratio of the portion of the splat that has not yet settled down. If the step does not continue with a gap (shown in Figure 5e) that can be covered by the splat, the splat breaks (Figure 5c) or covers the corner of the step (Figure 5d) according to the ratio and the height of the step. Otherwise, the gap is covered by the splat (Figure 5e), and a pore is formed. Pores formed in this way fall into the second and third categories of pore formation mechanisms mentioned in subsection 2.2.

4. If the splat encounters a dead end (Figure 5f), it first fills the available space and then flows over the outer surface if the volume of the remaining splat is great enough.

To successfully simulate the coating microstructure, several important parameters are used in these rules. According to the situations in which these parameters are used, there are five groups of parameters: (a) Two parameters are used to determine how deep the unmelted part of the particle penetrates into the gap (Figure 5b) depending on the width of the gap, and therefore, these two parameters determine the size of a macrosized pore. (b) In the third rule, when a splat meets a vertical drop step (Figure 5c and d), the ratio of the step height to the splat thickness determines whether the splat will break. (c) If the splat breaks when it meets a vertical drop step (Figure 5c), the distance that it breaks away is determined by an equation (with three adjustable parameters) that accounts for the thickness of the splat, the length of the splat that breaks, and the height of the step. (d) If the splat does not break when it meets a vertical drop step (Figure 5d), a pore forms at the corner of the step (the size of the pore is determined by a parameter that represents the slope of the splat covering the corner). (e) In the fourth rule, a necessary parameter is the slope of the bulk formed by the splat at the dead end (Figure 5f). All of these parameters were carefully selected according to considerations of their physical meaning and were tuned to provide results for important coating variables (such as coating porosity) that are consistent with the available experimental results.[8,10]

By means of these parameters, these four basic rules control how each particle hits and deforms on the substrate to form a lamellar-structured coating. The simulated coating structure can then be used to calculate the coating porosity and roughness. Specifically, the coating porosity P is calculated using the equation

$$P = \frac{n_1}{n_1 + n_2} \tag{8}$$

where n_1 is the number of void grids under the simulated coating surface and n_2 is the number of grids occupied by splats under the simulated coating surface. The deposition efficiency η is calculated using the equation

$$\eta = \frac{V_1}{V_1 + V_2} \tag{9}$$

where V_1 is the volume of the particles that are added to the coating and V_2 is the volume of the solid particles that are bouncing off by hitting the surface formed by unmelted particles. Note that all partially melted and fully melted particles stick to the surface independently of the nature of the coating layer at the hitting position.

3.3. Simulation Settings. The simulation model is based on the operation of the Diamond Jet Hybrid gun, whose geometric configuration can be found in the first article of this series.[21] Table 1 lists the baseline operat-

Table 1. Baseline Operating Conditions for the Diamond Jet Hybrid Thermal Spray Process Used in the Simulation

parameter	value
flow rate of oxygen, O_2 (scfh)	578
flow rate of propylene, C_3H_6 (scfh)	176
flow rate of air (scfh)	857
spray distance, L (mm)	245
characteristic diameter d_{10} (μm)	15
characteristic diameter d_{50} (μm)	35
characteristic diameter d_{90} (μm)	77
particle injection velocity, v_{p_0} (m/s)	20
width of the simulated coating section (μm)	819.2
desired set point of the coating thickness (μm)	254

Table 2. Thermophysical Properties of the Powder Particles

parameter	value
powder	nickel
density (kg/m^3)	8.9×10^3
melting temperature (K)	1727
heat capacity (J kg^{-1} K^{-1})	471
latent heat of melting (J/kg)	3×10^5
liquid kinematic viscosity (m^2/s)	6.2×10^{-7}

ing conditions (recommended by the manufacturer), the typical particle size distribution, and the dimension of the simulated coating section. In particular, the three characteristic diameters (d_{10}, d_{50}, and d_{90}) are listed as a reference for the log−normal distribution of the powder particles. When particles with different sizes are used in the simulation, these three characteristic diameters are varied proportionally, i.e., only one characteristic diameter is needed to describe a certain log−normal distribution of the particles. Therefore, we mention only d_{50} to characterize the size distributions of the various powders used in this paper. The physical properties of the particles used for coating formation are listed in Table 2.

The model simulates a section of the coating. The section is assumed to be a rectangle and is discretized by a 8192 × 4096 mesh. The size of each grid in the mesh is 0.1 × 0.1 μm. Such a grid size is about one-half of the height of the splat formed by a fully melted particle whose diameter is 40 μm under the baseline operating conditions. According to the mathematical model describing the gas and particle behavior,[21] particles whose size is smaller than about 8 μm are mostly fully unmelted. Thus, a grid size of 0.1 μm is small enough to carry out a simulation of coating growth with reasonable computing power. Each splat formed by a particle hitting the previously formed coating surface is discretized to a combination of grids and is placed on the coating surface by following certain rules (see subsection 3.2). Any splat with a thickness of less than 0.1 μm is rounded to 0.1 μm. Equation 10 shows the relationship between the ratio of splat diameter (D) and thickness (h) and the flattening degree (ξ)

$$\frac{D}{h} = 1.5\xi^3 \tag{10}$$

Usually, ξ is around 8 according to our calculations, which means that the splat diameter D is around 768 times the splat thickness h. Considering such a high particle deformation, a smaller grid size would not be able to substantially improve the accuracy of the computed results; this point was verified by running representative simulations with different grid size.

4. Simulation Results and Discussions

4.1. Microstructure of Coatings Made of Particles of Different Molten States. Under normal operating conditions, the gas temperature at the exit of the gun is around 2000 K, which is several hundred Kelvin higher than the melting point of a nickel particle. However, simulation results[21] show that, even at such a high temperature, only particles in a certain size range, about 10−40 μm, can be fully melted, whereas others, either too small or too large, are in a coexistence state of liquid and solid or even in a solid state at the point of impact on the substrate. The very small particles, although they might be totally melted during flight, are not in a fully molten state at impact because they are cooled quickly in the free jet as a result of the gas temperature decay and their small thermal inertias. The experiments of Zhang et al.[24] also have shown that particles at the point of impact on the substrate can be in different molten states (fully melted, partially melted, or solid) because of their different sizes and different trajectories in the HVOF thermal spray process. Figure 6 shows the simulated configuration of the coating sections that are perpendicular to the substrate for particles with different molten states. The simulated section in Figure 6a is formed by particles that are all fully melted (ideal case in which the particle velocity is calculated according to the baseline operating conditions and the particle melting ratio is assumed to be 1), whereas the one in Figure 6b is formed by particles with nonuniform molten states (some particles might be partially melted or even unmelted, in which case the particle velocity, temperature, and degree of melting are calculated according to the baseline operating conditions). The ideal lamellar structure of the thermally sprayed coating can be easily seen in Figure 6a. However, such a lamellar structure is disturbed by the unmelted part of the particles, as shown in Figure 6b. This figure also shows that large unmelted particles affect the coating surface dramatically, thus leading to a high coating roughness. To show the pore size and distribution inside of the coating, we construct Figure 6b again by ignoring the difference between each splat; the result is shown in Figure 6c. The white dots in Figure 6c represent the pores. He et al.[25] and Totemeier et al.[26] observed similar coating microstructures in their experiments. It can be concluded from this comparison that the particle melting behavior plays a very important role in the evolution of the coating microstructure and should be taken into account in the simulation model.

The effect of the particle melting behavior on the coating porosity was studied by analyzing the simulation results. Figure 7 shows the comparison of the coating porosity simulated by two different models. One model considers the particle melting behavior, i.e., the melting ratio of each particle is calculated by a mathematical model[21] that considers the particle size and the operating conditions. Another model assumes that all particles are fully melted but uses values for the other parameters, such as the particle velocity, that are calculated according to the same mathematical model.[21] The comparison shows the importance of considering the particle melting behavior, which has not been included in previous coating simulation models.[15−17] For the model considering that all the particles are fully melted, the coating porosity decreases monotonically as the particle size (d_{50}) increases, indicated by the dashed line

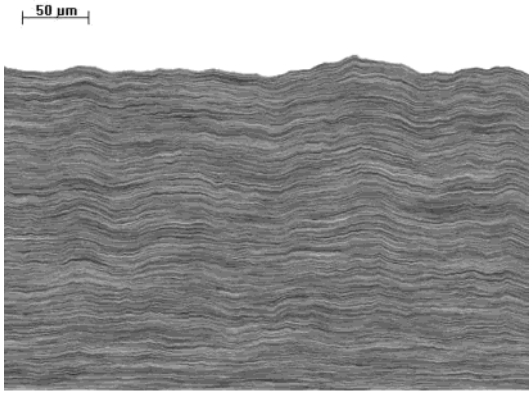

(a) Deposition of fully-melted particles - coating microstructure

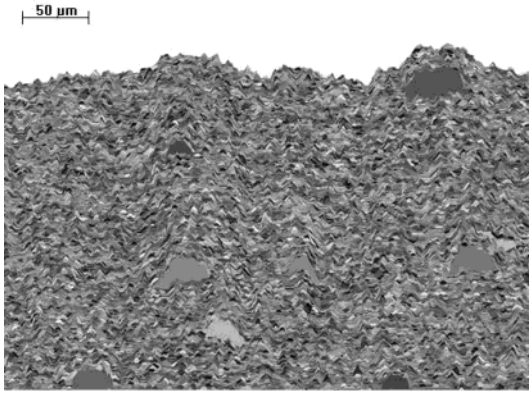

(b) Deposition of partially-melted particles - coating microstructure

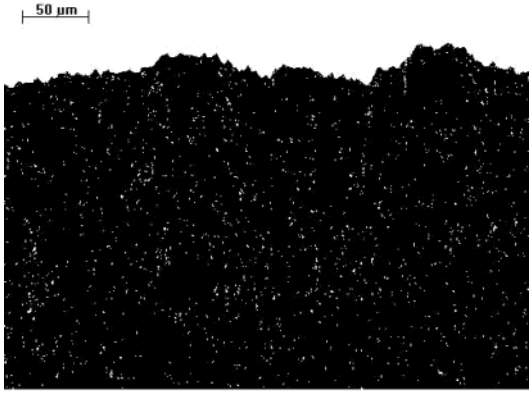

(c) Deposition of partially-melted particles - pore distribution

Figure 6. Simulated coating sections for fully melted particles and partially melted particles.

in Figure 7. However, the simulated coating porosity accounting for the particle melting behavior first decreases and then increases, as the particle size (d_{50}) increases, as indicated by the solid line in the same figure. The existence of a minimum porosity can be explained by the existence of the maximum particle melting ratio for particles with different sizes (Figure 8). Several experimental studies[8,10] have demonstrated that better particle melting conditions can lead to a lower coating porosity. It was also found that the error band increases as larger particles are used in the simulation. Such a phenomenon can be explained by the formation of more macropores when larger particles are

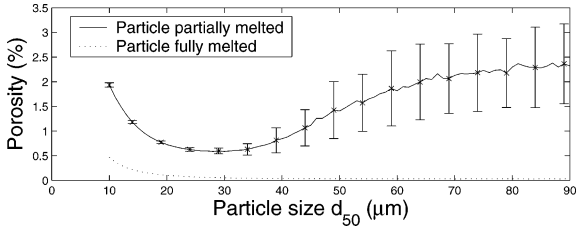

Figure 7. Comparison of simulation results for fully melted and partially melted particles under baseline operating conditions.

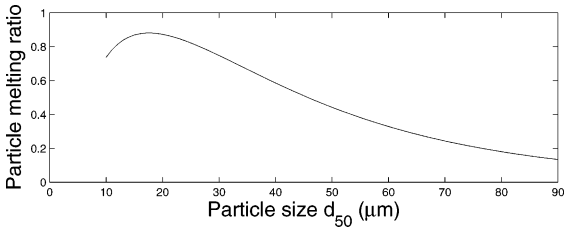

Figure 8. Melting ratios of particles with different sizes under baseline operating conditions.

used for the coating. Simulations show that the number of macropores is usually less than 50 inside one simulated coating section. Under operating conditions in which macropores strongly influence the coating porosity (e.g., when large particles are used to form the coating), a small change in the number of macropores strongly influences the coating porosity.

4.2. Influence of Operating Conditions on Coating Properties. In addition to providing useful insight into coating formation and growth, the developed model was used to make a comprehensive parametric analysis, which allows for the systematic characterization of the influence of operating conditions and the effect of the particle size on the coating porosity and deposition efficiency. The parametric analysis of the effects of the macroscopic operating conditions on the coating microstructure is based on the "one-factor-at-a-time" method, i.e., for each simulation, only one processing parameter is varied from 55 to 150% of its value under baseline conditions while all other parameters are fixed. The influence of the particle size on the coating microstructure was also studied by varying the powder size distribution parameters, i.e., d_{50} (whose corresponding cumulative weight function is 0.5), from 20 to 60 μm. The simulated results in the following figures are averages of a large number of repeated simulation runs performed under the same operating conditions to obtain a convergent average value and make the variance sufficiently small. The effects of variations in the process parameters are compared with the available experimental data in the following subsections.

4.2.1. Effect of the Oxygen Flow Rate. Figure 9 shows the influence of the oxygen flow rate and particle size on the particle melting ratio, coating porosity, surface roughness and deposition efficiency. Figure 9a reveals that the particle melting ratio increases significantly and becomes almost flat as the oxygen flow rate increases from its lower bound (318 scfh) to its upper bound (867 scfh); this behavior can be explained by the discussion in section 4 of the first article of this series.[21] When the oxygen flow rate is small, the equivalence ratio is far from its optimal value. As the oxygen flow rate increases, the equivalence ratio becomes close to its optimal value, and the combustion pressure increases (because of an increase in the total mass flow rate of

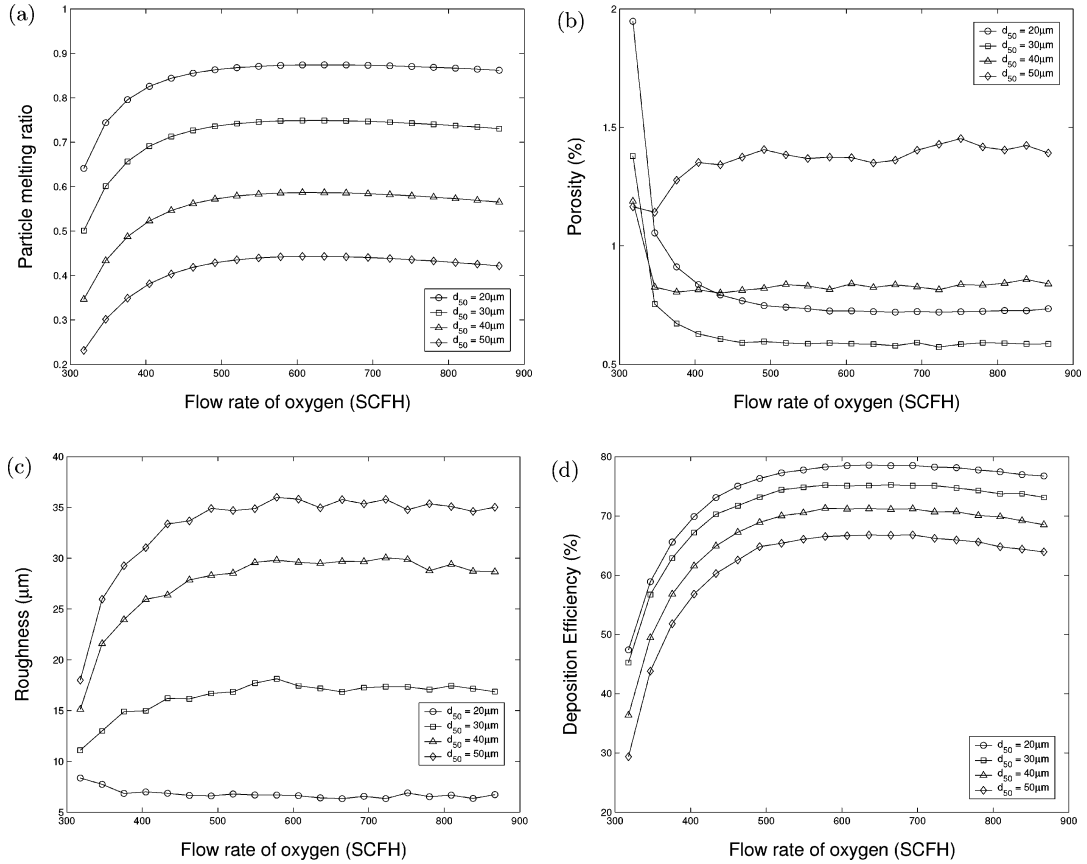

Figure 9. Effect of the oxygen flow rate on the particle melting behavior, coating porosity, surface roughness, and deposition efficiency.

the gas) at the same time. This leads to an increase of the gas temperature, and therefore, the particle temperature goes up sharply. However, after the oxygen flow rate exceeds a critical value at which the equivalence ratio departs significantly from its optimal value, the gas temperature slightly decreases. This is because the effect of an increase in the combustion pressure partially compensates for the effect of a decrease in the equivalence ratio. Accordingly, for particles of small size, the coating porosity decreases very rapidly initially and then approaches a nearly constant value as the oxygen flow rate spans its entire range of variation (Figure 9b). This implies that, for small particles, good particle melting conditions (i.e., higher degree of particle melting) help to decrease the coating porosity. For large particles, the coating porosity is high, which can be explained by the low melting ratio of large particles at the point of impact on the substrate, which results in large pores being formed in the coating structure. We should also note the effect of the particle size on the coating porosity. Figure 9b shows that a coating formed by a powder with $d_{50} = 30\ \mu$m has a lower porosity than a coating formed by a powder with $d_{50} = 20\ \mu$m. The roughness of the coating increases with the particle size, but it is not affected much by the oxygen flow rate, as shown in Figure 9c. This is because the coating roughness is controlled by the unmelted part of the particles, the amount of which does not change much as the oxygen flow rate changes. The effect of the oxygen flow rate on the deposition efficiency is similar to the effect on the particle melting ratio, as shown in Figure 9d. When the oxygen flow rate is less than 500 scfh, higher oxygen flow rates and smaller particle sizes lead to higher degrees of particle melting and higher deposition efficiencies.

4.2.2. Effect of the Fuel Flow Rate. Compared to the influence of the oxygen flow rate, variations in the fuel flow rate exhibit more obvious effects on the coating properties, as shown in Figure 10. For example, a peak in the fuel flow rate vs particle melting ratio can be clearly seen in Figure 10a. This is because the total mass flow rate does not increase much in the range of interest (because the flow rate of fuel is small compared to those of oxygen and air), and the gas temperature is a function of only the equivalence ratio. For particles of different sizes, the maximum melting ratio occurs when the fuel flow rate is about 210 scfh, whose corresponding equivalence ratio is about 1.2. Accordingly, as the fuel flow rate increases, the coating porosity first decreases and then increases, and the lowest coating porosity is achieved when the fuel flow rate is around 210 scfh. This fact further substantiates the point that good particle melting conditions (i.e., high degree of particle melting) are beneficial for achieving a lower coating porosity. However, particle melting is not the only factor affecting the coating porosity. Figure 10b shows that a coating formed by a powder with $d_{50} = 30\ \mu$m has a lower porosity than a coating formed by a powder with $d_{50} = 20\ \mu$m, although smaller particles experience better melting conditions than larger ones. This is similar to the observation in Figure 9b. Once again, the roughness of the coating increases with the particle size, and the relationship between the coating roughness and the fuel flow rate is not strong (Figure 10c). Consistent with the variation of the particle melting ratio, the deposition efficiency is shown to increase first and then decrease as the fuel flow rate increases (Figure 10d).

4.2.3. Effect of the Air Flow Rate. The effect of air, which partially functions as a coolant in the

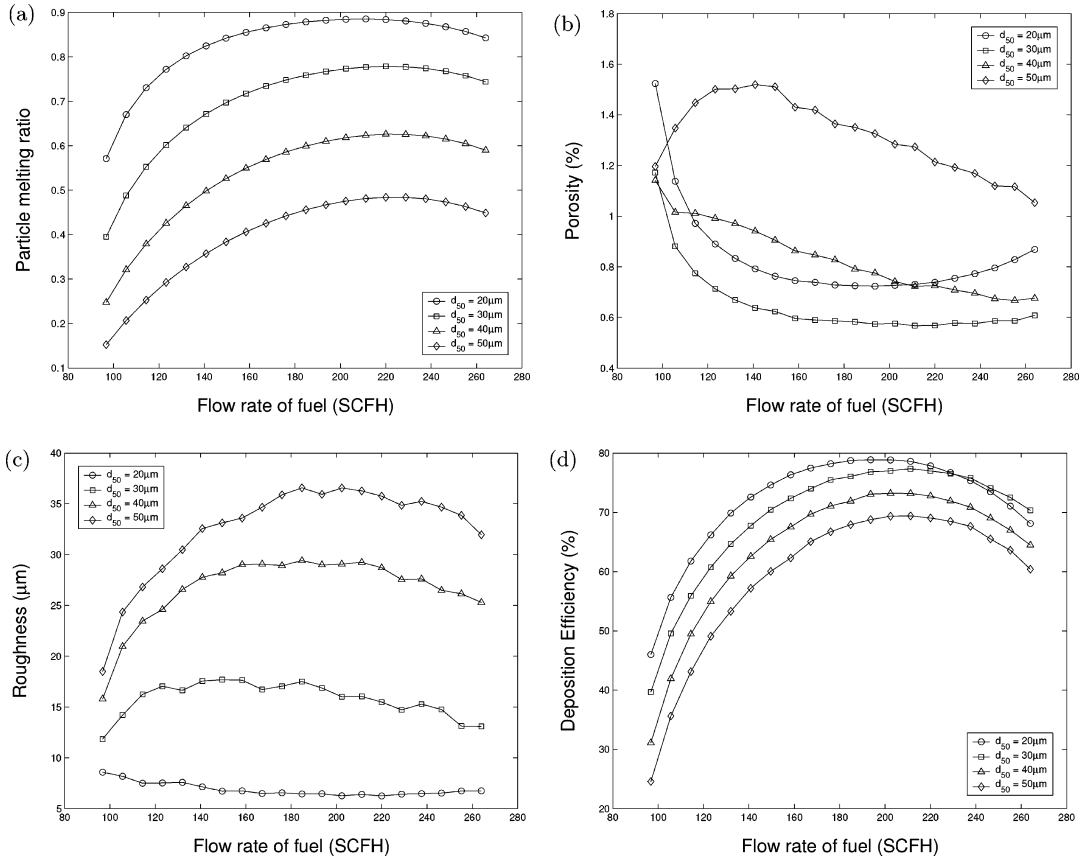

Figure 10. Effect of the fuel flow rate on the particle melting behavior, coating porosity, surface roughness, and deposition efficiency.

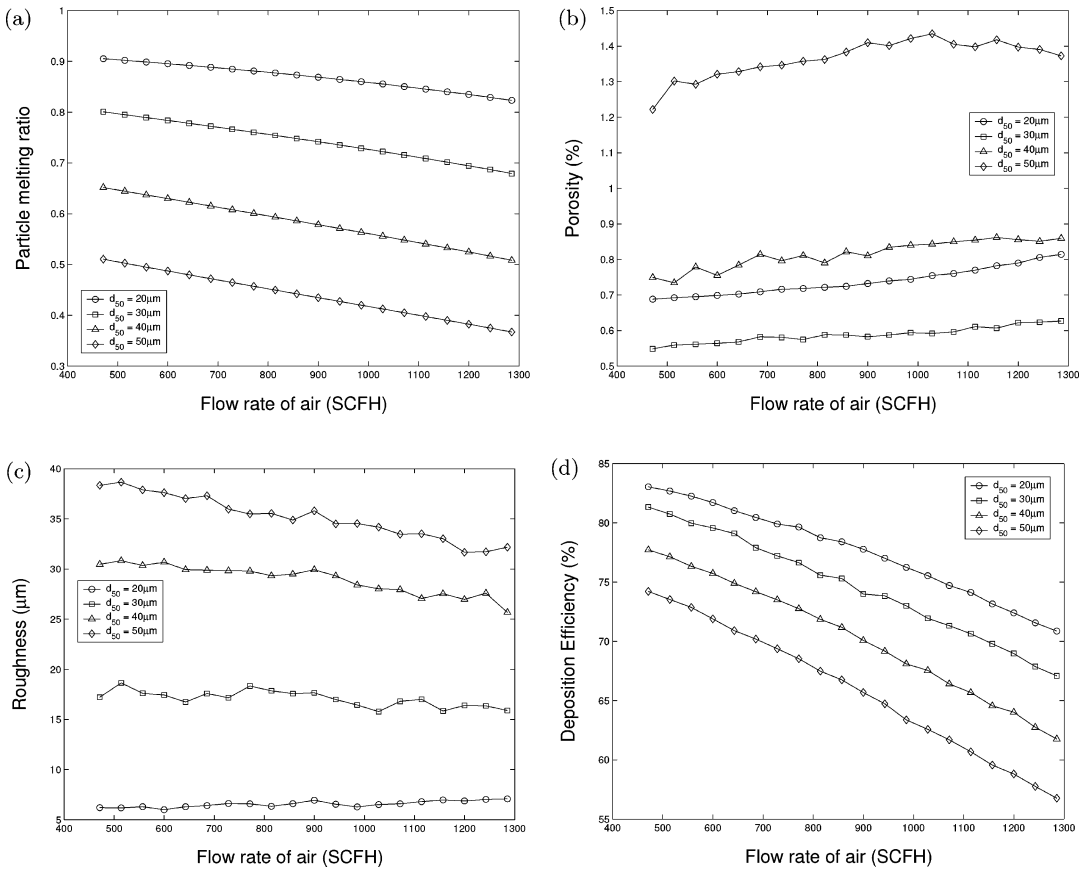

Figure 11. Effect of the air flow rate on the particle melting behavior, coating porosity, surface roughness, and deposition efficiency.

HVOF thermal spray process, can be seen in Figure 11. As the air flow rate increases, the particle melting ratio at the point of impact on the substrate decreases (Figure 11a). Correspondingly, the porosities of the coatings

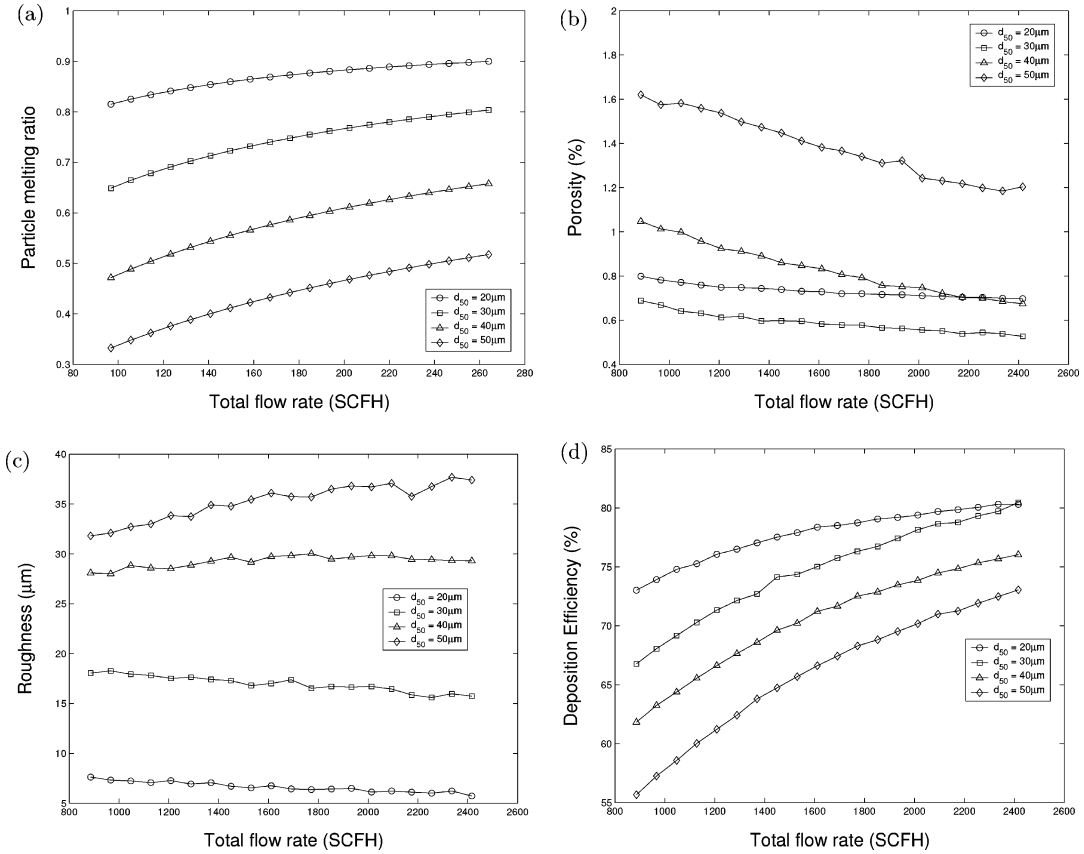

Figure 12. Effect of the total mass flow rate on the particle melting behavior, coating porosity, surface roughness, and deposition efficiency.

deposited by different-sized particles increase, as shown in Figure 11b. Regardless of the change in the air flow rate, the coating roughness is almost proportional to the particle size (Figure 11c). A higher air flow rate leads to a lower deposition efficiency (Figure 11d). Moreover, an increase in the particle size decreases the deposition efficiency.

4.2.4. Effect of the Total Mass Flow Rate. The effect of the total mass flow rate can be seen in Figure 12. According to Figure 12a, the relative ratio of the fuel, oxygen, and air flow rates is kept at the baseline conditions as the total mass flow rate varies from 50 to 150% of its baseline conditions. For different particle sizes, the particle melting ratio changes almost linearly with the total mass flow rate. Such a dependence is different from the corresponding effects of the fuel flow rate and of the oxygen flow rate. The increase in the degree of particle melting is caused by an increase in the combustion pressure and, therefore, in the gas temperature.[21] Note that, as the total mass flow rate increases, the particle velocity at the point of impact also increases.[21] From Figure 12b, it can be seen that the coating porosity decreases slowly as the total mass flow rate changes. This is caused by an increase in both the degree of particle melting and the impact velocity. The deposition efficiency increases dramatically as the total mass flow rate increases. Again, the coating formed by powder particles with a mean size of $d_{50} = 30\ \mu$m has the lowest porosity and almost the highest deposition efficiency, as shown in Figure 12d. Also, the coating roughness is mainly a function of the particle size and is almost independent of the total mass flow rate.

4.2.5. Effect of the Spray Distance. The spray distance has the most complicated effect on the particle melting behavior and coating porosity. Figure 13a shows that the particle melting ratio decreases as the spray distance increases. Furthermore, the melting ratio of smaller particles drops much faster than that of larger ones. For instance, the melting ratio of the particles with $d_{50} = 20\ \mu$m becomes even lower than that of the larger particles ($d_{50} = 40\ \mu$m) at large spray distances. As a result, the coating porosity generally increases as the spray distance increases, as shown in Figure 13b. Among all particle sizes of interest, the porosity of the coatings produced by particles with $d_{50} = 20\ \mu$m increases the fastest as the spray distance increases and becomes even the largest at a large spray distance. Figure 13c shows that the coating roughness is high at small spray distances, when the particle melting ratio is high, and decreases as the spray distance increases, especially for large particles. One possible reason for this behavior is that the deposition efficiency is less than 50% for large spray distances (shown in Figure 13d). Such a low deposition efficiency leads to the result that the increase in the number of unmelted particles bouncing off the surface outweighs the increase in the number of unmelted particles caused by the decrease of the particle melting ratio. Because only the melted part of the particles and small unmelted particles are deposited on the surface, small coating roughness can be achieved at long spray distances. Such a phenomenon can also be observed in Figures 9c and 10c. When the deposition efficiency is less than 50%, which is caused by low flow rates of oxygen and fuel, the coating roughness is also quite low. Figure 13d also shows that the deposition

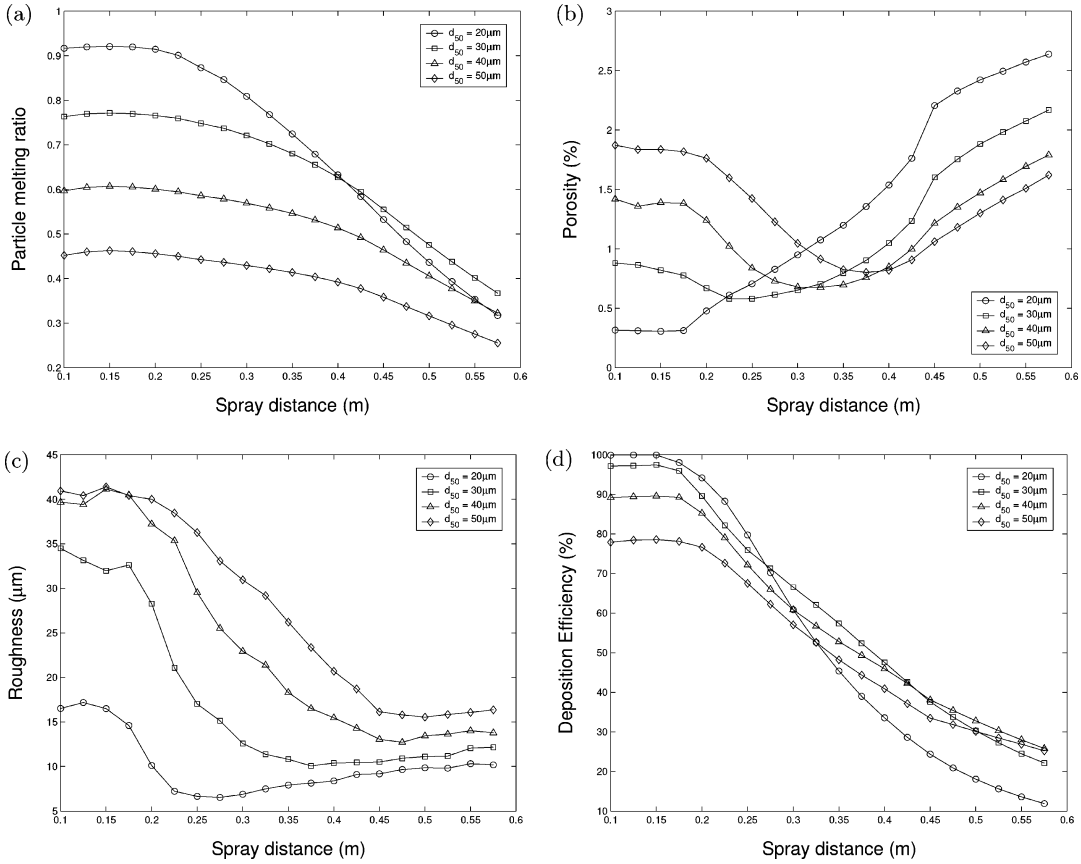

Figure 13. Effect of the spray distance on the particle melting behavior, coating porosity, surface roughness, and deposition efficiency.

Table 3. References of Available Experimental Results

ref	HVOF system	fuel	powder	size (μm)
Hearley et al.[10]	UTP TopGun	propylene	NiAl	15−45
de Villers Lovelock et al.[7]	JP-5000	kerosene	WC-17%Co	16−45
Gil and Staia[8]	JP-5000	kerosene	NiWCrBSi	22−66
Lih et al.[12]	A3000	propylene	CrC/20NiCr	
Lugscheider et al.[11]	diamond jet hybrid	hydrogen/propane	MCrAlY	
Gourlaouen et al.[9]	diamond jet hybrid	propylene	stainless steel	

efficiency decreases very rapidly because the particle melting ratio decreases significantly as the spray distance increases. Specifically, comparing the curves for small particles ($d_{50} = 20$ μm) in Figure 13a and d, we can see that, at large spray distances, the deposition efficiency for particles with $d_{50} = 20$ μm becomes the lowest among all the particles of interest, and their melting ratio is even less than that of larger particles. Such a result substantiates the conclusion that the particle melting condition has the strongest effect on the deposition efficiency.

4.3. Comparison of Stochastic Simulation Results and Experimental Studies. The influence of operating conditions on the coating microstructure and deposition efficiency have been experimentally studied by various groups.[7−12] The gun types and corresponding fuels and powders used in these HVOF thermal spray processes are listed in Table 3. In this subsection, we attempt to put the simulation results described above into perspective with respect to the available experimental results.

The significant effect of the equivalence ratio (which strongly affects the degree of particle melting) on the coating porosity has been analyzed by several experimental studies. For instance, the porosity of inert-gas-atomized (IGA) NiAl coatings produced by the UTP TopGun HVOF gun is 2% when the equivalence ratio is 1.26, which is close to the optimal value.[21] When the equivalence ratio is maintained at 1.68, which is far from the optimal value, the porosity is 2.54% (or 3.38%) as a result of the increasing fuel flow rate (or decreasing oxygen flow rate).[10] Although the equivalence ratio is the same in the latter two cases, the coating porosity is higher when the total mass flow rate is lower, which validates the conclusion drawn in subsection 4.2.4. Conducting experiments on NiWCrBSi coating processing using a JP-5000 HVOF thermal spray system, Gil and Staia[8] pointed out that the best coating properties are achieved at an equivalence ratio between 1.1 and 1.2, which is very close to our prediction. Note that, although a liquid fuel (kerosene) is used in this process, the relationship between the equivalence ratio and the combustion temperature (see analysis in the work of Swank et al.[27]) is very similar to that of the Diamond Jet hybrid HVOF thermal spray process studied in our work.[21]

One of the main conclusions of our study is that better particle melting conditions (higher degree of particle melting, which occurs under fuel-rich conditions) increase the deposition efficiency. This conclusion is

substantiated by the experiments of Hearley et al.,[10] who found that, when the equivalence ratio gets close to the optimal value and the total gas flow rate increases, the deposition efficiency also increases. Sakaki and Shimizu[28] also drew such a conclusion on the basis of their experimental studies. By analyzing the effects of the gun size on HVOF thermal spray, they found that a higher degree of particle melting leads to a higher deposition efficiency.

5. Conclusions

Judging from the above discussion of the influence of operating conditions on coating microstructure and deposition efficiency, the following main conclusions can be drawn:

1. Particle melting behavior plays a very important role in determining the coating microstructure. A high degree of particle melting tends to achieve a low coating porosity and a high deposition efficiency. This requires the system to be operated under fuel-rich conditions ($\varphi = 1.2$ for the Diamond Jet Hybrid thermal spray process).

2. Particle size has a significant effect on the coating porosity. Particles with a mean size (d_{50}) of around 35 μm tend to achieve the lowest coating porosity among all of the particles of interest here under various operating conditions, including fuel-rich conditions. Furthermore, the larger the particle size, the higher the coating surface roughness.

In summary, the comparison of simulation results and available experimental data shows that the stochastic simulation model developed here can be used to properly predict the effects of process parameters, including the particle size; spray distance; and flow rates of oxygen, fuel, and air, on the microstructure of the coatings produced by the Diamond Jet hybrid HVOF thermal spray process.

Acknowledgment

Financial support from a 2001 Office of Naval Research Young Investigator Award, program manager Dr. Lawrence Kabacoff, is gratefully acknowledged.

Notation

A = area of the splat (m^2)
d = diameter of the particle (m)
D = diameter of the splat (m)
h = height of the coating (m)
i = index
L = length of the simulated coating section (m)
n = number of grid points
Pr = Prandtl number
R_a = roughness (m)
Re = Reynolds number
u = random number uniformly distributed in [−0.5, 0.5]
v = velocity (m/s)
w = random number uniformly distributed in [−0.5, 0.5]
We = Weber number
x = coordinate of the direction parallel to the simulated coating section
y = coordinate of the direction perpendicular to the simulated coating section

Greek Letters

ξ = flattening ratio
ν = kinematic viscosity of the droplet (m^2/s)
ρ = density (kg/m^3)
ϵ = thermal diffusivity of the solidified layer (m^2/s)
σ = surface tension of the droplet (kg/s^2)

Superscripts and Subscripts

m = melted
p = properties related to the particle
um = unmelted

Literature Cited

(1) Pawlowski, L. *The Science and Engineering of Thermal Spray Coatings*; John Wiley & Sons: Chichester, U.K., 1995.

(2) Cheng, D.; Trapaga, G.; McKelliget, J. W.; Lavernia, E. J. Mathematical modeling of high velocity oxygen fuel thermal spraying: an overview. *Key Eng. Mater.* **2001**, *197*, 1.

(3) Cheng, D.; Xu, Q.; Trapaga, G.; Lavernia, E. J. A numerical study of high-velocity oxygen fuel thermal spraying process. Part I: Gas-phase dynamics. *Metall. Mater. Trans. A* **2001**, *32*, 1609.

(4) Li, M.; Christofides, P. D. Feedback control of HVOF thermal spray process accounting for powder size distribution. *J. Therm. Spray Technol.*, in press.

(5) Li, M.; Christofides, P. D. Modeling and analysis of HVOF thermal spray process accounting for powder size distribution. *Chem. Eng. Sci.* **2003**, *58*, 849.

(6) Christofides, P. D. *Model-Based Control of Particulate Processes*; Particle Technology Series; Kluwer Academic Publishers: Dordrecht, The Netherlands, 2002.

(7) De Villiers Lovelock, H. L.; Richter, P. W.; Benson, J. M.; Young, P. M. Parameter study of HP/HVOF deposited WC−Co coatings. *J. Therm. Spray Technol.* **1998**, *7*, 97.

(8) Gil, L.; Staia, M. H. Influence of HVOF parameters on the corrosion resistance of NiWCrBSi coatings. *Thin Solid Films* **2002**, *420−421*, 446.

(9) Gourlaouen, V.; Verna, E.; Beaubien, P. Influence of flame parameters on stainless steel coatings properties. In *Thermal Spray: Surface Engineering via Applied Research, Proceedings of the 1st International Thermal Spray Conference*; Berndt, C. C., Ed.; ASM International: Materials Park, OH, 2000; p 487−493.

(10) Hearley, J. A.; Little, J. A.; Sturgeon, A. J. The effect of spray parameters on the properties of high velocity oxy-fuel NiAl intermetallic coatings. *Surf. Coat. Technol.* **2000**, *123*, 210.

(11) Lugscheider, E.; Herbst, C.; Zhao, L. Parameter studies on high-velocity oxy-fuel spraying of MCrAlY coatings. *Surf. Coat. Technol.* **1998**, *108−109*, 16.

(12) Lih, W.-C.; Yang, S. H.; Su, C. Y.; Huang, S. C.; Hsu, I. C.; Leu, M. S. Effects of process parameters on molten particle speed and surface temperature and the properties of HVOF CrC/NiCr coatings. *Surf. Coat. Technol.* **2000**, *133*, 54.

(13) Chen, Y.; Wang, G.; Zhang, H. Numerical simulation of coating growth and pore formation in rapid plasma spray tooling. *Thin Solid Films* **2001**, *390*, 13.

(14) Cirolini, S.; Harding, J. H.; Jacucci, G. Computer simulation of plasma-sprayed coatings: I. Coating deposition model. *Surf. Coat. Technol.* **1991**, *48*, 137.

(15) Knotek, O.; Elsing, R. Monte Carlo simulation of the lamellar structure of thermally sprayed coatings. *Surf. Coat. Technol.* **1987**, *32*, 261.

(16) Ghafouri-Azar, R.; Mostaghimi, J.; Chandra, S.; Charmchi, M. A stochastic model to simulate the formation of a thermal spray coating. *J. Therm. Spray Technol.* **2003**, *12*, 53.

(17) Mostaghimi, J.; Chandra, S.; Ghafouri-Azar, R.; Dolatabadi, A. Modeling thermal spray coating processes: a powerful tool in design and optimization. *Surf. Coat. Technol.* **2003**, *163*, 1.

(18) Liu, H.; Lavernia, E. J.; Rangel, R. H. Numerical simulation of substrate impact and freezing of droplets in plasma spray processes. *J. Phys. D: Appl. Phys.* **1993**, *26*, 1900.

(19) Liu, H.; Lavernia, E. J.; Rangel, R. H. Numerical stimulation of impingement of molten Ti, Ni, and W droplets on a flat substrate. *J. Therm. Spray Technol.* **1993**, *2*, 369.

(20) Liu, H.; Lavernia, E. J.; Rangel, R. H. Modeling of molten droplet impingement on a nonflat surface. *Acta Metall. Mater.* **1995**, *43*, 2053.

(21) Li, M.; Shi, D.; Christofides, P. D. Diamond jet hybrid HVOF thermal spray: Gas-phase and particle behavior modeling and feedback control design. *Ind. Eng. Chem. Res.* **2004**, *43*, 3632−3652.

(22) Madejski, J. Solidification of droplets on a cold surface. *Int. J. Heat Mass Transfer* **1976**, *19*, 1009.

(23) Mellali, M.; Fauchais, P.; Grimaud, A. Influence of substrate roughness and temperature on the adhesion/cohesion of alumina coatings. *Surf. Coat. Technol.* **1996**, *81*, 275.

(24) Zhang, D.; Harris, S. J.; McCartney, D. G. Microstructure formation and corrosion behaviour in HVOF-sprayed Inconel 625 coatings. *Mater. Sci. Eng. A* **2003**, *344*, 45.

(25) He, J.; Ice, M.; Lavernia, E. J. Particle melting behavior during high-velocity oxygen fuel thermal spraying. *J. Therm. Spray Technol.* **2001**, *10*, 83.

(26) Totemeier, T. C.; Wright, R. N.; Swank, W. D. Microstructure and stresses in HVOF sprayed iron aluminide coatings. *J. Therm. Spray Technol.* **2002**, *11*, 400.

(27) Swank, W. D.; Fincke, J. R.; Haggard, D. C.; Irons, G. HVOF gas flow field characteristics. In *Proceedings of the 7th National Thermal Spray Conference*; Berndt, C. C., Sampath, S., Eds.; ASM International: Materials Park, OH, 1994; pp 313−318.

(28) Sakaki, K.; Shimizu, Y. Effect of the increase in the entrance convergent section length of the gun nozzle on the high-velocity oxygen fuel and cold spray process. *J. Therm. Spray Technol.* **2001**, *10*, 487.

(29) Lau, M. L.; Jiang, H. G.; Nuchter, W.; Lavernia, E. J. Thermal Spraying of Nanocrystalline Ni Coatings. *Phys. Status Solidi A: Appl. Res.* **1998**, *166*, 257.

(30) Crow, E. L.; Shimizu, K. *Log−Normal Distributions: Theory and Applications*; Marcel Dekker: New York, 1988.

Received for review July 3, 2003
Revised manuscript received October 9, 2003
Accepted October 10, 2003

IE030560H